J Solid State Electrochem (2009) 13:619–631
DOI 10.1007/s10008-008-0761-6

ORIGINAL PAPER

Electrochemical polarisation and galvanic couple behaviour of the primary phase of 55% Al–Zn coating investigated using band microelectrodes (BME) and band microelectrode arrays

Troy A. Lowe · Gordon G. Wallace · Aaron K. Neufeld

Received: 16 September 2008 / Revised: 27 November 2008 / Accepted: 2 December 2008 / Published online: 18 December 2008

Abstract Electrochemical polarisation experiments have shown that anodic dissolution processes on Al–40% Zn alloys are significantly enhanced in chloride compared to sulfate-based electrolytes. The aluminium content of the alloys allowed passive behaviour to be observed in sulfate electrolyte even in the presence of zinc-rich precipitates on the surface. Electrolyte pH affected cathodic processes, which was attributed to the rate of proton reduction and the passivity of the surface. Monitoring the OCP of the alloy band during polarisation of neighbouring zinc electrodes in band microelectrode (BME) arrays showed that generation of alkaline pH at the zinc electrodes affected the OCP of the alloy when the inter-electrode spacing was 10, 50, and 200 μm. Where elements of a BME array were close enough to interact via mass transport, the overall galvanic behaviour of the cell was found to be anodic or cathodic, whereas the alloy was consistently cathodic with respect to zinc in galvanic cells at larger separations.

Keywords Corrosion · Al–Zn alloy · Zinc · Aluminium · Microstructure · Electrochemical polarisation · Galvanic couple

Introduction

The continued development of corrosion-resistant surface coatings to extend the life of steel products is important in terms of economic value and optimising the use of our finite resources [1]. Zinc is widely used to provide galvanic protection of steel from corrosion in automotive applications, structural materials, roofing, and other domestic and industrial applications [2]. Al–Zn alloy metal coatings such as 5% Al–Zn (Galfan®) and 55% Al–Zn (known as Galvalume in the US, Zincalume® steel in Australasia and AluZinc in Europe) offer a significant improvement in corrosion performance in some service environments over galvanised steel [3, 4].

The microstructure of 55% Al–Zn alloy coating has been well characterised [5–8]. The coating contains a primary, aluminium-rich, dendritic phase (α-phase) containing approximately 65 wt.% Al, 35 wt.% Zn. and 0.2 wt.% Si that occupies about 80% of the surface with a dendrite arm spacing (DAS) of around 10 μm. The interdendritic volume or β-phase (mainly a eutectic) contains approximately 95% zinc, about 4 wt.% aluminium and less than 1 wt.% silicon. The microstructure is a consequence of a complex solidification sequence; however, it can be simplified somewhat as follows. Interfacial Al–Fe–Si–Zn alloy forms at the steel surface followed by solidification of α-phase in the overlay, forming dendrites supersaturated with zinc and containing fine zinc precipitates. Solidification of β-phase proceeds as a 5% Al–Zn eutectic within the interdendritic regions interspersed with α-phase, iron intermetallics, and

Dedicated to the 80th birthday of Keith B. Oldham.

T. A. Lowe · G. G. Wallace (✉)
ARC Centre of Excellence for Electromaterials Science,
Intelligent Polymer Research Institute, University of Wollongong,
Northfields Avenue,
Wollongong, NSW 2522, Australia
e-mail: gwallace@uow.edu.au

A. K. Neufeld (✉)
BlueScope Steel Limited,
Old Port Road,
Port Kembla, NSW 2505, Australia
e-mail: Aaron.Neufeld@bluescopesteel.com

larger silicon particles, the latter residing near the quaternary alloy layer.

Examination of 55% Al–Zn alloy-coated steel after atmospheric exposure in industrial, rural, and marine test sites from a number of studies indicates that corrosion commences in the zinc-rich β-phase [5, 9–11], and it is generally accepted that the improved corrosion performance compared to galvanised coatings is attributed to the accumulation and retention of corrosion products within channels that exists between the dendrites, on the surface of the metal coating [12], and on exposed steel at a cut edge or defect [13, 14]. SRET and SVET studies by McMurray, Worsley and coworkers [15, 16] demonstrated that multiple coactive anodic sites on the surface of a 55% Al–Zn coating, generating localised current densities of 100–200 μA cm^{-2}, deactivated relatively quickly after initiation. The number of sites and their lifetime decreased with increasing amount of aluminium in the overlay; however, a profoundly different microstructure is implicit with a variation of aluminium at levels of 0.1%, 4.3% and 55%, making the direct comparisons between these compositions less meaningful. Ex situ microscopic inspection also revealed localised dezincification from the β-phase of the coating [15, 16].

The results of electrochemical-based studies of galvanised (Zn–0.1% Al), Zn–4.3% Al, 55% Al–Zn-coated steel, and pure zinc have been reported [17–19]. With respect to the oxygen reduction processes, the conclusions emphasise diffusion-limited oxygen reduction and facile dissolution kinetics at the β-phase of 55% Al–Zn coating, similar to that of pure zinc [20]. Based on the high aluminium content, an unsubstantiated assumption is made in these studies that the α-phase makes negligible contribution to reduction processes. Unusually high cathodic current densities on the 55% Al–Zn coating measured by Dafydd et al. are rationalised by a plausible but not verified existence of some catalytic effect imparted by iron intermetallics known to reside within the eutectic [18]. Proton reduction has also been observed on the 55% Al–Zn coating in low pH conditions [14]. The high overpotential for proton reduction on zinc would suggest that this process occurs at aluminium-rich sites; however, the location, temporal persistence and kinetics of these processes needs to be better evidenced and quantified.

So, it remains that the electrochemistry of the α-phase alone, which occupies about 80% of the 55% Al–Zn overlay volume in the form of dendrites and an equally high proportion of the surface area, is poorly understood. There is a significant body of work devoted to the role of intermetallic phases in commercially relevant aluminium alloys, and one successful approach in this area has been the synthesis of model intermetallic phases and subsequent electrochemical characterisation and galvanic coupling of these with the matrix alloy [21–23].

A distinct challenge in the study of the α-phase is producing a model alloy with the same composition and microstructure as that which comprises the dendrites in the metal coating overlay. A reasonable sized ingot of Al–40% Zn that may be used to construct an electrode with a conventional size could have shrinkage voids even though steps are taken to minimise porosity. Considering the low solubility of zinc in aluminium, the microstructure of a cast alloy would also display distinct and course precipitation of zinc within the solid solution of Al–Zn alloy even after patient heat treatment and rapid cooling. The notion that compositional inhomogeneity would have a strong influence on the electrochemical corrosion behaviour of the alloy is not unreasonable given the behaviour of many of the aluminium alloys that contain hardening precipitates [24–27]. Preparation of thin foils from a cast structure was undertaken in the current study to allow for faster heat treatment and a much more effective quench, producing a highly refined microstructure and chemically homogeneous alloy.

Given that the preparation of foils lends itself to the construction of microelectrodes and microelectrode arrays, it is relevant to consider the theoretical descriptions of the diffusion-limited response of band-shaped microelectrodes. Rigorous theoretical descriptions of the diffusion to microelectrodes of various geometries and experimental conditions are available, the most relevant to this work being those describing processes at a single band microelectrode [28–34] or band microelectrode array [35–39]. Of common interest is to determine the theoretical chronoamperometric response and resulting concentration profile for the electrodes, which is usually done by computational and analytical techniques [40–44]. Oldham's seminal paper on edge effects at inlaid electrodes provided a general analytical solution for the current density as well as the concentration profile at any inlaid electrode undergoing a diffusion limited potential-step type experiment [45]. Oldham's result may be applied to band electrodes with the limitation that the model becomes inaccurate when $4\sqrt{Dt}$ exceeds the width or a limit of $t=10$ s given a width of 400 μm and $D=1\times10^{-5}$ cm^2 s^{-1}. This solution overestimates the current density at narrower band electrodes [30, 46] such as those used in the current work; however, the solution is straightforward to implement and provides an upper boundary for the concentration change expected during an experiment under diffusion control such as oxygen reduction. Figure 1 shows the calculated concentration profile along a surface away from the perimeter of an inlaid electrode (hatched) where C is the theoretical concentration and C_a is the concentration of a reaction product at the electrode. The diffusion coefficient was taken as $D=1\times10^{-5}$ cm^2 s^{-1}. The calculation suggests that

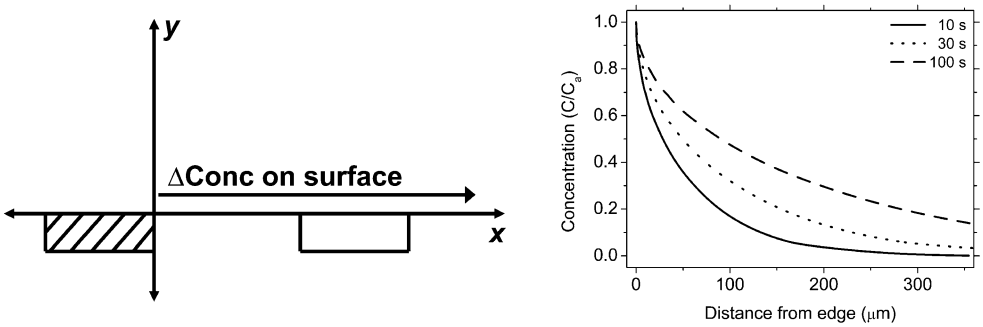

Fig. 1 Diagram showing two inlaid band electrodes (*left*) and normalised concentration (*right*) at y=0 as a function of distance from an electrode edge for a diffusion limited process

as the spacing of the two bands (hatched and open) is increased, the second electrode will experience a significantly reduced concentration of the electrogenerated product. Based on this model, BME arrays in the current work were constructed with a central band consisting of Al–40% Zn alloy flanked by two parallel zinc bands (optical image shown in Fig. 2), with spacings of 10, 50, 200 and 4000 μm to accommodate overlapping diffusion fields of varying extent.

Microelectrodes and microelectrode arrays using inert metals as an electrode material have often been used as probes in corrosion studies, [47–52] but less attention has been paid to constructing a microelectrode from the active metal of interest [53–56]. In the current paper, electrochemical polarisation data of BMEs constructed from Al–40% Zn alloys, high purity zinc and high purity aluminium in Na_2SO_4 and NaCl at pH 4, neutral pH, at pH 10, and in dilute Harrison's solution (DHS) are presented. The effect of electrode spacing on the galvanic interaction between heat-treated Al–40% Zn alloy and pure zinc was explored by conducting galvanic coupling experiments using BME arrays prepared with a range of inter-electrode distances.

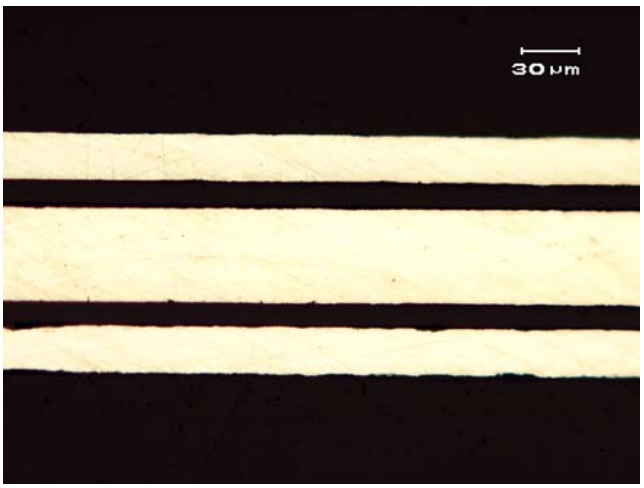

Fig. 2 Optical microscope image of a BME array in plan view containing a central, 50-μm-wide Al–40% Zn alloy band flanked by two 25-μm-wide Zn bands, separated by 10 μm

Experimental

Al–40% Zn alloy was prepared by melting 60 wt.% Al and 40 wt.% Zn at 600 °C and casting into ingots, which were then heat treated at 450 °C for 6 h and quenched. Foils of the Al–40% Zn alloy were prepared by cold-rolling a 500-μm thick slice of the cast alloy into foils ca. 50-μm thick. Homogenisation of the microstructure was achieved by further heat-treating the foils at 400 °C for 1 h and quenching in water. The microstructure of the alloys was characterised using a Hitachi S3400-N scanning electron microscope (SEM). Images of the rolled alloy and heat-treated alloy are shown in Fig. 3. High purity Zn (99.99%) and Al (99.999%) foils were obtained from Goodfellow.

BMEs were prepared by mounting multiple foils spaced approximately 4 mm apart in a cold-set epoxy resin (Struers EpoFix). Each of the foils were individually connected to a five-pin electrical connector also mounted in epoxy. The cross-section of each foil was exposed by plane grinding and polishing the end of the cylindrical epoxy block. To specifically probe the galvanic interaction between Al–40% Zn alloy and zinc, foils of these metals were positioned in a close proximity arrangement (10–200 μm). These assemblies were constructed by compressing a central 50-μm wide Al–40% Zn alloy band in between two 25-μm wide bands of zinc, separated by PET film of the desired thickness. An electrical connection was made to each of the bands individually. An optical microscope image of a BME array with 10 μm spacing is shown in Fig. 2. Prior to electrochemical experiments, the electrode–epoxy mounts were plane ground using #1200 and #4000 SiC paper (Struers) lubricated with water and then polished using 3 μm diamond polish and an non-aqueous based lubricant (Struers, Yellow). The polished surface was cleaned with ethanol, patted dry with a tissue and left for 10 min in air at ambient prior to experiments.

All electrochemical corrosion measurements were made using a VMP potentiostat (Biologic-Science Instruments).

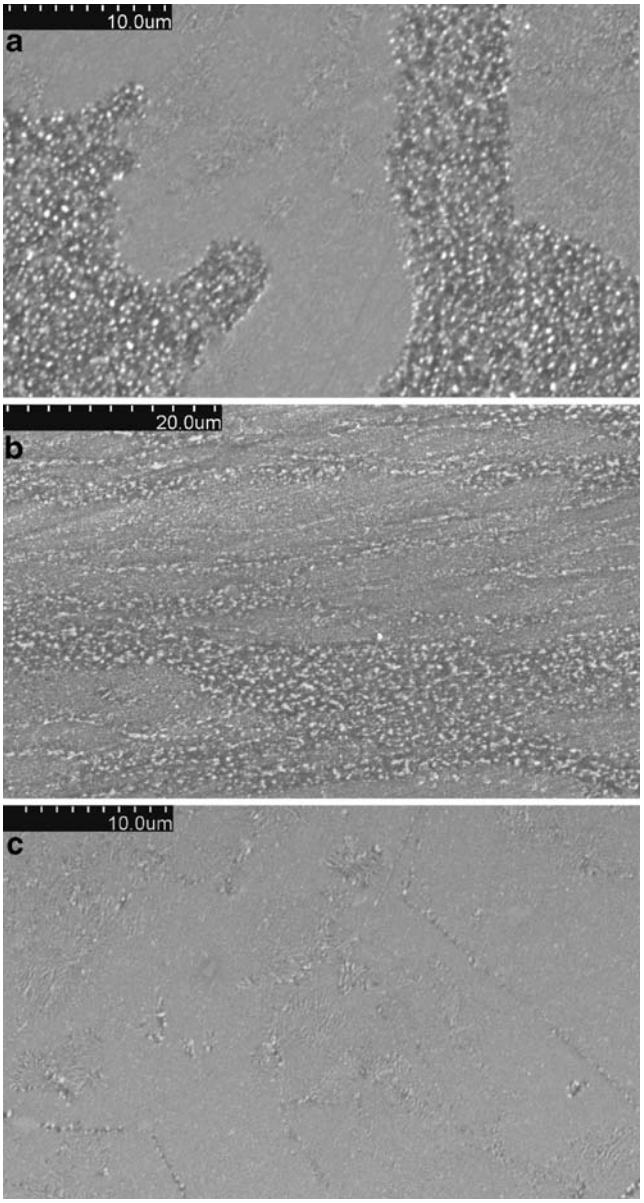

Fig. 3 SEM images of Al–40% Zn alloy: **a** as cast, **b** after rolling and **c** after rolling and heat treatment. Obtained in backscattered electron imaging mode

Potentiodynamic experiments were conducted in 0.1 M Na_2SO_4, 0.1 M NaCl and a mixture of 0.0265 M $(NH_4)_2SO_4$ and 0.00856 M NaCl, commonly known as dilute Harrison's solution (DHS), using AR grade reagents (Sigma Aldrich). Neutral Na_2SO_4 and NaCl solutions had a pH between 6.0 and 6.5, while DHS had a pH between 5.0 and 5.5. Concentrated H_2SO_4 and HCl were used to adjust the Na_2SO_4 and NaCl electrolytes, respectively, to pH 4, and NaOH to shift the pH of both sulfate and chloride electrolytes to pH 10. Electrolytes were aerated for at least 20 min prior to the start of experiments. The working electrode was left for 10 min at open circuit prior to the potential sweep experiments, then the potential was swept at a rate of 1.667 mV s^{-1}. A cathodic sweep of the potential involved polarisation from +0.015 V versus OCP to −1.5 or −1.8 V, an anodic sweep of the potential from −0.015 V versus OCP to −0.7 V. Different from the aforementioned "single-sided" potentiodynamic experiment, a traditional full sweep of the potential ranged from −1.5 V (−1.8 V at pH 10) to −0.5 V. Polarisation data were recorded in triplicate on one or more of the BMEs mounted in a single epoxy mount simultaneously using the NSTAT mode with a single Ag|AgCl (3.5 M KCl) reference and platinum counter electrode. All electrode potentials quoted in this report are referenced to Ag|AgCl (3.5 M KCl). Where possible, the corrosion current (I_{corr}) was calculated by extrapolating the Tafel slopes from the anodic or cathodic branches of single-sided polarisation curves to the corrosion potential (E_{corr}).

The galvanic current between BMEs of varying spacing was measured by coupling the heat-treated Al–40% Zn alloy and the zinc bands in zero-resistance ammeter (ZRA) mode. As a matter of convention, the Al–40% Zn alloy was connected to the potentiostat as the working electrode. Hence, a positive current indicated oxidation of the alloy and a negative current reduction processes where dominating. The open circuit potential (OCP) of both sets of BMEs was measured for 10 min upon immersion, followed by a 16-h period measuring the couple current and cell potential and a 10-min open circuit measurement at the end.

Results

Microstructure of binary Al–40% Zn alloy

The microstructure of the cast and rolled forms of the Al–40% Zn alloy are shown in Fig. 3. As cast (Fig. 3a), the alloy may be described as having three components, (1) a uniform phase that has a chemical composition of about Al–20% Zn, (2) a regular but heterogeneous phase that has an average composition about Al–40% Zn but contains small (<5 μm diameter) zinc rich particles, and (3) irregularly distributed larger zinc rich particles that are greater than 5 μm in diameter. The partition of the uniform and heterogeneous domains is about even. When rolled, these domains are literally smashed together, the result is a striated mixture of course and fine zinc-rich particles (Fig. 3b). Fig. 3c shows the rolled Al–40% Zn alloy after heat treatment and quench. This resulted in a metastable supersaturated solid-solution of zinc in aluminium, which decomposed over time (10–15 days at room temperature) into a two-phase system unlike that observed in the cast or rolled samples. Initially this manifested as very small zinc-

rich precipitates 0.1 to 0.3 μm in diameter (Fig. 3c), generally localised to the boundaries of grains that were 20 to 30 μm in size. After 20 to 30 days, a high density of zinc-rich precipitates up to 0.5 μm in length were observed to occupy entire grains, while the majority of the remaining surface (about 70%) of the band maintained a homogeneous dispersion of zinc in aluminium (not shown). Electrochemical experiments involving the heat-treated Al–40% Zn alloy were conducted within 10 days of heat treatment to best capture the microstructure that resembles the α-phase contained in a 55% Al–Zn coating (Fig. 3c).

Electrochemical polarisation of Al–40% Zn alloys, high purity Zn and Al

Electrochemical polarisation experiments were conducted on both the heat-treated and rolled forms of the Al–40% Zn alloy to investigate the influence of microstructure, while experiments were conducted on pure zinc and aluminium to understand the influence of the component metals and the role that their distinctly different passive films have on anodic and cathodic processes. Results of polarisation experiments of BMEs constructed from heat-treated and rolled Al–40% Zn alloys, in all electrolytes and pH conditions are shown in Figs. 4, 5 and 6. Polarisation experiments on BME composed of high purity aluminium and zinc are shown in Fig. 7. E_{corr} and I_{corr} values extracted from the electrochemical polarisation data for all electrolytes and pH values are given in Tables 1 and 2.

E_{corr} of the heat-treated Al–40% Zn alloy in Na_2SO_4 were around −0.74 V at pH 4 and 0.92 V at neutral, while at pH 10, the E_{corr} values were around −1.18 V. Noteworthy is the evolution of the OCP from the time of immersion at −1.03 V to about −0.73 V after 10 min. The E_{corr} estimated from the full potential sweep experiment at pH 4 was −0.61 V, 100 mV positive of E_{corr} measured from anodic and cathodic sweeps, while at neutral, the effect is the opposite, and the full sweep the E_{corr} is about 100 mV more negative. In NaCl electrolyte, the electrolyte pH had less of an influence compared to that with Na_2SO_4. The E_{corr} values were around −0.94 V at pH 4 and −0.97 V at neutral pH, while at pH 10, the E_{corr} values were around −1.15 V.

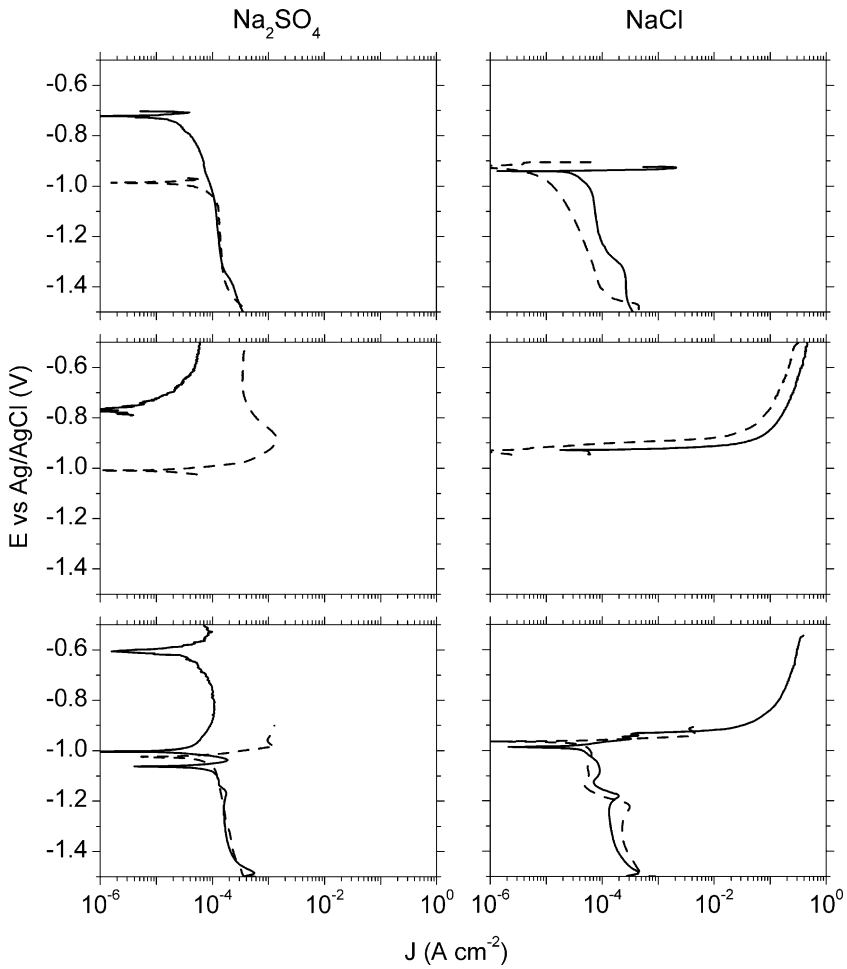

Fig. 4 Representative polarisation curves of BME constructed from heat-treated Al–40% Zn alloy (*solid*) and rolled Al–40% Zn alloy (*dashed*) in 0.1 M Na_2SO_4 (*left*) and 0.1 M NaCl electrolytes (*right*) adjusted to pH 4. Sweep range: cathodic (*top*), anodic (*centre*) and full sweep (*bottom*) are shown

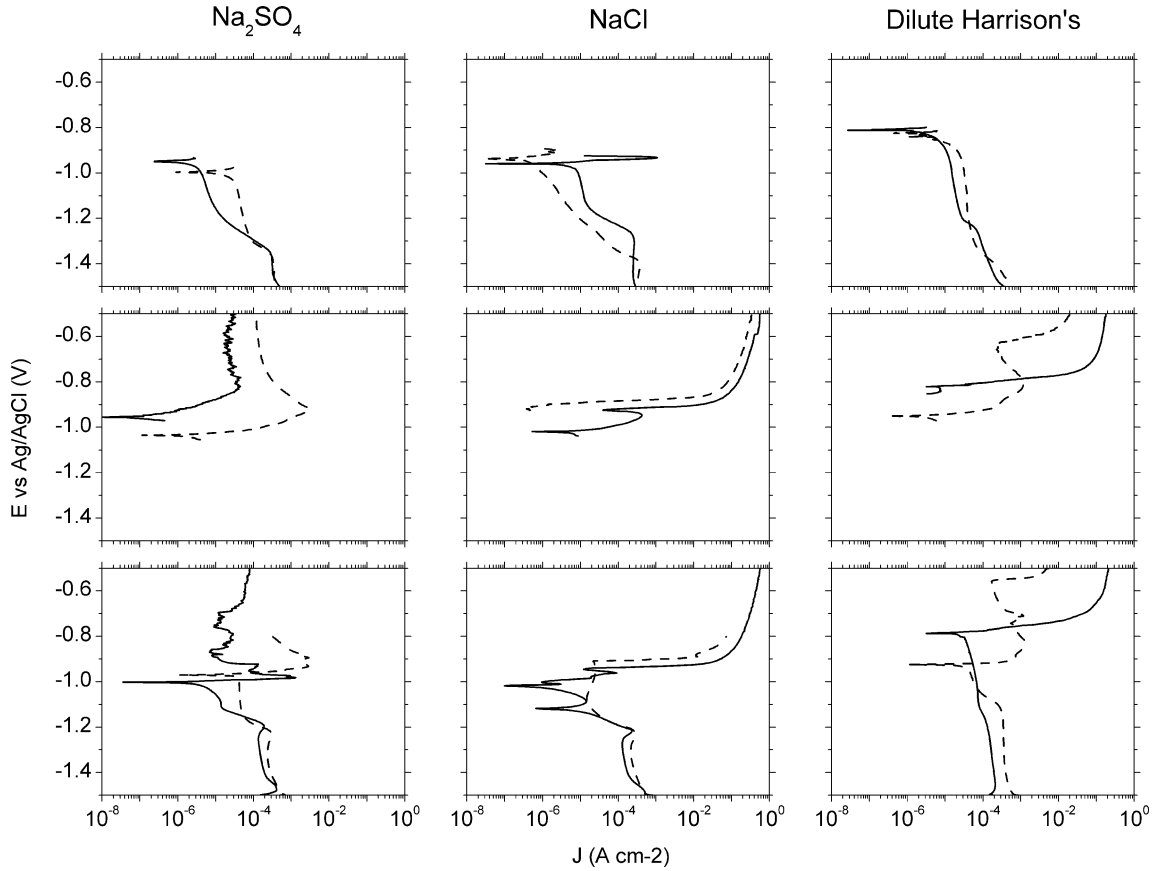

Fig. 5 Representative polarisation curves of BME constructed from heat-treated Al–40% Zn alloy (*solid*) and rolled Al–40% Zn alloy (*dashed*) in 0.1 M Na_2SO_4 (*left*), 0.1 M NaCl (*middle*) and DHS (*right*) at neutral pH. Sweep range: cathodic (*top*), anodic (*middle*) and full sweep (*bottom*) are shown

In DHS, the E_{corr} was about −0.83 V, with a slight positive shift to −0.79 V when conducting the full potential sweep. Upon immersion in DHS, the OCP of the homogeneous Al–40% Zn alloy was around −1.03 V, shifting to a more positive potential of about −0.85 V over the 10-min open circuit period, similarly to the behaviour observed in Na_2SO_4 at pH 4.

In all electrolytes, the E_{corr} obtained from anodic and cathodic "single-sided" potential sweeps were within about 20 mV, whilst values obtained from full sweep experiments varied. Furthermore the full sweep experiments occasionally resulted in polarisation curves where the current changed polarity more than once, such as in Na_2SO_4 at pH 4, giving the impression of multiple E_{corr} values on the log J vs E plots. In this case, the system is not at steady state, and so, it is not meaningful to report E_{corr} and I_{corr} data. Another instance of non-steady state conditions was for the full sweep in neutral NaCl. In this case, reduction processes did not dominate the net current; however, the oxidative current approached the detection limit of the potentiostat and then increased again at slightly more positive potentials.

I_{corr} of heat-treated Al–40% Zn alloy at pH 4 and pH 10 had values in the range 2.0 to 6.4×10^{-6} A cm^{-2}, while in neutral, Na_2SO_4 I_{corr} were between about 0.3 and 0.5×10^{-6} A cm^{-2}. In NaCl, I_{corr} values were markedly higher at pH 4 and neutral compared to Na_2SO_4; however, at pH 10 and in DHS, I_{corr} were similar.

Cathodic polarisation behaviour of heat-treated Al–40% Zn alloy were similar in Na_2SO_4 and NaCl at pH 4 and pH 10, with a slightly higher limiting cathodic current density in NaCl at pH 4. In neutral electrolytes, the cathodic polarisation curves in both NaCl and Na_2SO_4, exhibited two diffusion limited current plateaus, the first close to 1×10^{-5} A cm^{-2} and the second around 3×10^{-4} A cm^{-2}. In DHS, the second plateau in the cathodic polarisation curve displayed a slightly lower current density at about 1×10^{-4} A cm^{-2}. The anodic polarisation curves of the heat-treated Al–40% Zn alloy were very different in NaCl, Na_2SO_4, and DHS. In Na_2SO_4 at pH 4, current density initially displayed Tafel behaviour near E_{corr} and then asymptotically approached 6×10^{-3} A cm^{-2}, while at neutral pH, the anodic current density fluctuated at around 2×10^{-3} A cm^{-2}. In Na_2SO_4 at pH 10, the alloy showed a

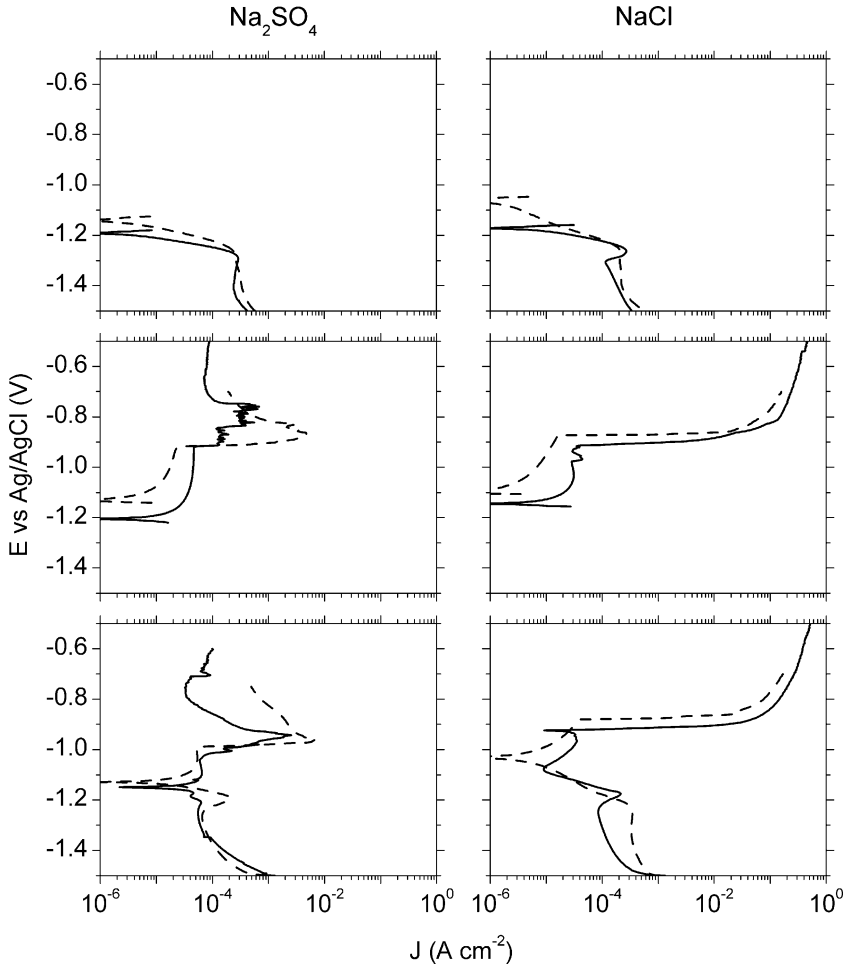

Fig. 6 Representative polarisation curves of BME constructed from heat-treated Al–40% Zn alloy (*solid*) and rolled Al–40% Zn alloy (*dashed*) in 0.1 M Na_2SO_4 (*left*) and 0.1 M NaCl electrolytes (*right*) adjusted to pH 10. Sweep range: cathodic (*top*), anodic (*middle*) and full sweep (*bottom*) are shown

stable oxidation current density of about 6×10^{-3} A cm^{-2} with a rapid increase in current density at −0.9 V and then repassivation at about −0.7 V. In NaCl at pH 4 and at neutral pH, the anodic current density was four orders of magnitude higher than observed in Na_2SO_4, displaying a rapid increase in oxidation current density immediately positive of the corrosion potential in a manner comparable to the anodic polarisation curves of pure zinc in NaCl. At pH 10, the anodic curve showed a gradual increase in current density from E_{corr} to −0.9 V, then a rapid increase in current density of five orders of magnitude. In DHS, the rapid increase in oxidation current was similar to that observed in neutral NaCl, but it was observed at a more positive potential of −0.8 V.

In contrast to the heat-treated Al–40% Zn alloy, E_{corr} of the rolled alloy in Na_2SO_4 electrolyte was around −1.00 V at pH 4 and neutral, and −1.14 V at pH 10. The same trend was observed in NaCl electrolyte, albeit the E_{corr} was 50 to 100 mV more positive. E_{corr} of rolled Al–40% Zn alloy depended less on electrolyte pH than the heat-treated form of the alloy. I_{corr} of the rolled Al–40% Zn alloy varied somewhat between the anodic, cathodic, and full sweep experiments. In pH 4 Na_2SO_4, the I_{corr} was an order of magnitude higher than in NaCl, which was the opposite trend to that observed for the heat-treated alloy. In neutral and pH 10 electrolytes, the I_{corr} determined from the anodic and cathodic polarisation sweeps were typically around 1×10^{-6} A cm^{-2} for all three electrolytes and an order of magnitude higher for the full sweeps, much like the values determined for the heat-treated form of the alloy.

The current densities and shape of cathodic polarisation curves of the rolled Al–40% Zn alloy were similar to the heat-treated Al–40% Zn alloy at pH 4 and pH 10 in both NaCl and Na_2SO_4. In neutral Na_2SO_4, the first cathodic current density plateau for the rolled alloy was an order of magnitude higher than the heat-treated alloy, while the curves were very similar, negative of −1.3 V where the second plateau began. In neutral NaCl, the cathodic current densities were approximately an order of magnitude lower than the heat-treated alloy and did not display the current density plateaus observed for the heat-treated alloy. In DHS, the cathodic behaviour was similar to the heat-treated alloy, with the first diffusion limited plateau extending to approximately −1.35 V rather than −1.2. In Na_2SO_4 at

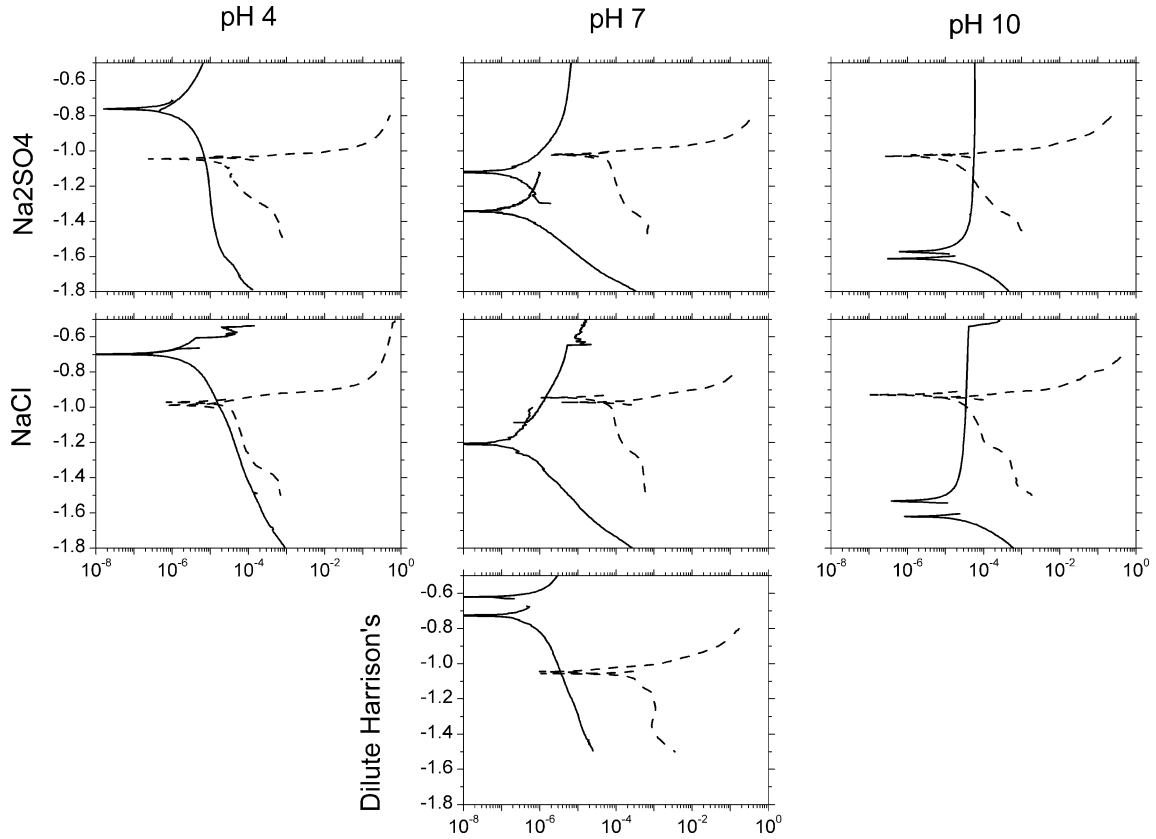

Fig. 7 Representative cathodic and anodic polarisation curves of BME constructed from (*solid*) high-purity aluminium and high-purity zinc (*dashed*) in pH 4 (*left*), neutral (*middle*) and pH 10 electrolytes (*right*) containing 0.1 M Na_2SO_4 (*top*), 0.1 M NaCl (*middle*) and DHS (*bottom*)

neutral and pH 4, there was a current density peak immediately positive of E_{corr} which tailed off to a steady-state current density of around 10^{-4} A cm^{-2}. SEM images of the surface following polarisation revealed dealloying of the large zinc-rich precipitates (Fig. 8). At pH 10, the anodic polarisation curve in Na_2SO_4 was similar to that of the heat-treated alloy, showing a rapid current increase at −0.90 V and corresponding decrease at −0.70 V. The anodic

Table 1 E_{corr} (V vs Ag|AgCl) determined from polarisation data of BMEs

		pH 4		pH 6.5		pH 5.0	pH 10	
		Na_2SO_4	NaCl	Na_2SO_4	NaCl	DHS	Na_2SO_4	NaCl
HT alloy	Ox	−0.76	−0.93	−0.94	−0.99	−0.83	−1.19	−1.15
	Red	−0.72	−0.94	−0.90	−0.95	−0.82	−1.18	−1.16
	Full	–[a]	−0.99	−1.02	–[a]	−0.79	−1.15	−0.93
Rolled alloy	Ox	−1.00	−0.93	−1.04	−0.89	−0.96	−1.14	−1.08
	Red	−0.98	−0.92	−1.00	−0.94	−0.82	−1.14	−1.07
	Full	−1.03	−0.97	−0.98	−0.97	−0.92	−1.13	−1.03
Zn	Ox	−1.04	−0.99	−1.02	−0.98	−1.05	−1.02	−0.94
	Red	−1.05	−0.97	−1.02	−0.95	−1.06	−1.02	−0.94
	Full	−1.05	−1.03	−1.00	−1.04	−1.06	−1.01	−1.00
Al	Ox	−0.76	−0.69	−1.12	−1.09	−0.61	−1.57	−1.54
	Red	−0.78	−0.68	−1.35	−1.20	−0.74	−1.61	−1.63
	Full	−0.87	−0.92	−1.15	−1.14	−0.75	−1.58	−1.49

[a] Not at a steady state, no E_{corr} defined

Table 2 I_{corr} (μA cm^{-2}) determined from polarisation data of BME's

		pH 4		pH 6.5		pH 5.0	pH 10	
		Na_2SO_4	NaCl	Na_2SO_4	NaCl	DHS	Na_2SO_4	NaCl
HT alloy	Ox	2.0	50	0.29	4.8	2.9	3.7	2.8
	Red	6.4	17	0.47	2.8	2.2	2.6	4.2
	Full	–[a]	0.092	4.4	–[a]	15	13	57
Rolled alloy	Ox	20	0.96	0.98	1.02	2.4	1.6	1.2
	Red	10	2.5	6.7	0.25	2.7	2.5	1.3
	Full	33	15	30	12	17	9.0	3.4
Zn	Ox	37	4.8	11	33	17	18	28
	Red	1.9	6.4	9.9	5.8	36	2.9	3.9
	Full	30	18	8.1	2.2	35	10	19
Al	Ox	0.54	0.33	0.071	0.39	0.13	5.6	3.1
	Red	0.23	1.4	0.074	0.072	0.12	2.6	6.1
	Full	0.068	0.054	0.080	0.061	0.048	6.7	14.2

[a] Not at a steady state, no E_{corr} defined

polarisation curves for the rolled alloy were similar to those observed for the heat-treated alloy and zinc in NaCl at all pH values. In DHS, anodic polarisation of the rolled alloy resulted in a current density peak of 10^{-3} A cm^{-2} at −0.80 V followed by a passive region and an increase in current density more positive of −0.60 V.

E_{corr} measured from polarisation of high purity zinc BME were in the range −0.94 to −1.06 V for all electrolytes and pH values. The E_{corr} values in NaCl were consistently 20 to 80 mV more positive than those measured in Na_2SO_4, while the values measured in DHS were the most negative at −1.05 V. I_{corr} of Zn were consistently higher than measured for the other electrode materials in this study, although the rolled alloy showed similar values in Na_2SO_4 electrolytes. The anodic and cathodic behaviour of zinc was consistent in all electrolytes, displaying diffusion-limited oxygen reduction plateaus in the cathodic branches and a sharp current density increase to over 0.1 A cm^{-2} immediately positive of E_{corr}.

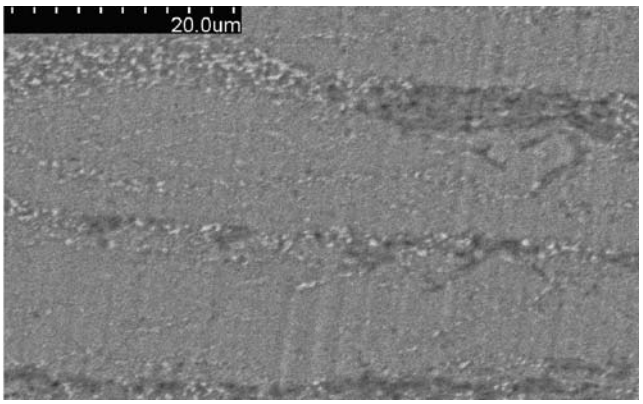

Fig. 8 Secondary electron image of rolled Al–40% Zn alloy after anodic polarisation in 0.1 M Na_2SO_4 electrolyte adjusted to pH 4

E_{corr} of the high-purity aluminium BME were strongly dependent upon pH, varying from −0.7 V at pH 4 to −1.6 V at pH 10. In neutral electrolyte, E_{corr} values of aluminium varied significantly (−1.00 to −1.36 V) as did the OCP prior to polarisation, consistent with values quoted in literature for aluminium in neutral Na_2SO_4 [57]. E_{corr} values were generally more positive in NaCl than Na_2SO_4 by 50 to 100 mV, while in DHS, E_{corr} were −0.6 to −0.75 V, similar to pH 4 NaCl and Na_2SO_4. I_{corr} of high purity aluminium were the lowest of all the materials used here save for at pH 10. All cathodic polarisation curves for high purity aluminium were at least one order of magnitude lower in current density than the other materials, except in NaCl at pH 4. The cathodic curves were flat and featureless, the current density rising as the potential was scanned more negative than about −1.45 V. The anodic polarisation scans were also generally, flat, featureless and at least an order of magnitude lower than the other materials. In neutral NaCl electrolyte, a rapid but relatively small increase in the current density was observed close to −0.65 V for the anodic and full sweep polarisation experiments.

Interaction of heat-treated Al–40% Zn alloy and zinc

The zinc elements of variably spaced BME arrays were polarised cathodically using a remotely placed platinum counter electrode while the OCP of the heat-treated Al–40% Zn alloy was monitored. During this type of experiment, the OCP of both the alloy and zinc were recorded initially, while the OCP of the Al–40% Zn alloy continued to be monitored while sweeping the potential of the zinc bands to −1.5 V. The changes in OCP of the Al–

Table 3 Change in the electrode potential (mV) relative to the open-circuit value of the heat-treated Al–40% Zn alloy during polarisation of Zn bands from OCP to −1.5 V in neutral 0.1 M Na_2SO_4 electrolyte

Element spacing (μm)	Zn band electrode potential				
	−1.1 V	−1.2 V	−1.3 V	−1.4 V	−1.5 V
10	+21	+30	−226	−277	−313
50	+31	+67	−54	−196	−243
200	−32	−10	−18	−90	−77
4,000	−19	−2	+38	+69	+82
Separate electrodes	+28	+48	+50	+145	+154

40% Zn alloy bands are shown in Table 3. There was a negative step change in the OCP of the Al–40% Zn alloy of around 300 mV for the 10 and 50 μm-spaced arrays (−0.95 to −1.25 V) when the potential of the zinc electrodes passed −1.2 and −1.24 V, respectively. This potential of the zinc electrodes corresponds to a transition from an oxide-covered to a bare zinc surface, and a change from a two-electron to a four-electron oxygen reduction mechanism [20]. A smaller negative shift in potential of around 100 mV was observed for the Al–40% Zn alloy in the array spaced at 200 μm, as the potential of the zinc electrode became more negative than −1.34 V. The OCP of the alloy in the array spaced at 4,000 μm and in the separate electrode shifted 80 to 150 mV more positive over the course of the experiment. A similar polarisation experiment configuring one of the zinc bands as the counter electrode resulted in the OCP of the Al–40% Zn alloy remaining around −0.95 V for the duration of the experiments for both the 10 and 50 μm spaced arrays.

A potential-step type experiment applying −1.4 V to the zinc bands of variably spaced BME arrays was also conducted. Evolutions of the OCP values for the Al–40% Zn alloy during experiments are shown in Table 4. A negative step change in the OCP of the Al–40% Zn alloy electrode accompanied the potential step of the zinc bands for the arrays spaced at 10, 50 and 200 μm whose magnitude decreased as the band spacing increased. The OCP of the Al–40% Zn alloy in the arrays at 10 and 50 μm remained relatively constant throughout the duration of zinc polarisation, while the OCP of the alloy in the array with 200 μm spacing drifted 220 mV more positive during the same period. Following polarisation, the OCP of the alloy in these three arrays shifted to values more positive of their initial OCP, while the OCP of the alloy in the array spaced at 4,000 μm and in the separated electrode cell shifted slightly positive over the course of the experiment.

Galvanic couple experiments between Al–40% Zn alloy and pure zinc BMEs prepared as separated mounts as well as BME arrays spaced from 10 to 4,000 μm in neutral Na_2SO_4 and NaCl electrolyte were conducted. Average results from these experiments are summarised in Tables 5 and 6 for Na_2SO_4 and NaCl electrolytes, respectively, while a graph showing a selection of galvanic currents (I_{cell}) in neutral Na_2SO_4 at all electrode spacings is shown in Fig. 9. The E_{cell} generated by the BME arrays spaced at 10 and 50 μm in Na_2SO_4 electrolyte started at ca. −1.12 and −1.06 V, respectively, changing to around −1.03 V over 4 h and remaining there for the duration of the experiment. The arrays spaced at larger distances typically displayed E_{cell} values within 20 mV of −1.03 V throughout the couple period. In NaCl electrolyte, the E_{cell} values were 60 mV more positive than those in Na_2SO_4 at −0.97 V. I_{cell} for the arrays spaced at 10, 50 and 200 μm displayed both positive and negative current densities in both electrolytes, at times changing polarity over the duration of the experiment, as shown for the 200-μm spaced array in Fig. 9. Conversely, the array spaced at 4,000 μm and the couple assembled from single BMEs in separate mounts consistently displayed negative galvanic current that increased in magnitude over the duration of the couple period and did not change polarity.

Discussion

The electrochemical polarisation behaviour of Al–40% Zn alloy

The interaction of the heat-treated alloy with sulfate ions hindered the anodic processes compared to the rolled alloy and pure zinc. This effect was more pronounced in acidic

Table 4 Average change in the electrode potential relative to the open circuit value of the heat-treated Al–40% Zn alloy during potential-step experiments on the Zn bands at open circuit for 1 min, followed by −1.4 V for 4 min then a 5-min open-circuit period in neutral 0.1 M Na_2SO_4 electrolyte

Element spacing (μm)	E (V) 60 s OCP	ΔE (mV) 40 s pol	ΔE (mV) 180 s pol	ΔE (mV) 150 s OCP	ΔE (mV) 300 s OCP
10	−1.054	−270	−283	+17	+130
50	−1.030	−177	−160	+41	+92
200	−0.989	−116	+114	+190	+199
4,000	−1.078	+11	+74	+138	+149
Separate electrodes	−1.018	+26	+76	+210	+247

Table 5 Summary of the average cell behaviour during 16 h galvanic coupling of the zinc elements with the central band of Al–40% Zn alloy in neutral 0.1 M Na_2SO_4 electrolyte

Band spacing (μm)	Ave couple current density (μA cm^{-2})		Overall range (μA cm^{-2})	E_{cell} (V)
	0–4 h	4–16 h		
10	0	−10	30 to −20	−1.03[a]
50	10	50	0 to 60	−1.03[a]
200	−50	20	40 to −120	−1.03
4000	−20	−40	0 to −70	−1.03
Separate electrodes	−45	−135	0 to −200	−1.03

For convention, positive current density values indicates that the Al–40% alloy is the anode, and zinc is the cathode.
[a] Values were −1.12 and −1.06 V for the 10- and 50-μm-spaced arrays, respectively, at the commencement of coupling and changed to −1.03 V after 4 h

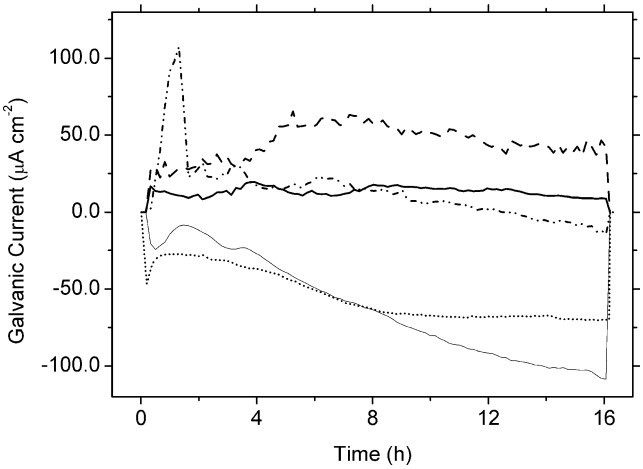

Fig. 9 Graph of the galvanic current arising between heat-treated Al–40% Zn alloy and high-purity zinc in BME arrays spaced at 10 μm (*dark solid*), 50 μm (*dash*), 200 μm (*dash dot dot*), 4,000 μm (*dot*) and separate mounts (*light solid*) in neutral 0.1 M Na_2SO_4 electrolyte. For convention, the Al–40% Zn alloy was configured as the working electrode in all experiments

than neutral or alkaline electrolytes and may be responsible for the change in OCP of the heat-treated alloy observed over the first few minutes after immersion in acidic sulfate electrolyte. The higher anodic current densities in chloride electrolyte for the Al–40% Zn alloys indicates that chloride ions accelerate the corrosion, presumably by the solubilisation of corrosion products and the transport of metal ions through surface oxides [58, 59]. This behaviour may contribute to the high galvanic protection ability of the 55% Al–Zn coating observed in the initial stages of corrosion in chloride electrolytes by Yadav et al. [14]. The cathodic branches of both heat-treated and rolled forms of the Al–40% Zn alloys displayed higher current densities at low overpotential compared to pure zinc at low pH, which may be due to a contribution of proton reduction to the cathodic current, which is kinetically hindered on pure zinc. The high cathodic current density of the Al–40% Zn alloys compared to aluminium may result from the passivity of the aluminium oxide film, which would be significantly disrupted by the zinc content of both forms of the alloy. The more negative E_{corr} in alkaline compared to neutral electrolytes for both forms of the Al–40% Zn alloy is a consequence of the aluminium content of the alloys. The higher solubility of aluminium oxides and the higher cathodic current densities observed for the Al–40% Zn alloys in alkaline electrolytes may be responsible for this.

Table 6 Summary of the average cell behaviour during 16 h galvanic coupling of the zinc elements with the central band of Al–40% Zn alloy in neutral 0.1 M NaCl electrolyte

Band spacing (μm)	Ave couple current density (μA cm^{-2})		Overall range (μA cm^{-2})	E_{cell} (V)
	0–4 h	4–16 h		
10	−40	0	30 to −90	−0.96
50	10	0	50 to −25	−0.98
200	140	110	30 to 200	−0.96
4,000	−35	−140	0 to −210	−0.97
Separate electrodes	−50	−60	0 to −140	−0.97

For convention, positive current density values indicates that the Al–40% alloy is the anode, and zinc is the cathode

The fact that the E_{corr} and I_{corr} values for the rolled alloy and pure zinc are similar is attributed to the presence of active zinc-rich islands in the rolled alloy, which is further evidenced by the dealloying observed after anodic polarisation (Fig. 8). The lower current densities displayed by the rolled alloy compared to zinc during anodic polarisation in sulfate electrolytes indicates that a stable passive film may be present in regions of the surface not occupied by the active zinc rich sites.

The positive E_{corr} and positive open-circuit drift observed during the OCP period of the Al–40% Zn alloys in DHS correlates with a lower pH and sulfate content in the electrolyte, while the facile anodic dissolution of the heat-treated form of the alloy is a consequence of the chloride in the electrolyte. However, the behaviour of the alloy in this electrolyte is not straightforward, as shown by the unusual anodic behaviour of the rolled alloy and the higher cathodic current density of zinc compared to results in chloride and sulfate electrolytes at neutral and acidic pH.

Polarisation and galvanic experiments on BME arrays

Polarisation experiments carried out using the zinc electrodes while monitoring the OCP of the central Al–40% Zn band of BME arrays highlight the capacity for band

electrodes (25 μm width) to significantly influence the nearby chemical environment on the tens of microns length scale. Results of cathodic potentiodynamic polarisation using a remote counter electrode show that the reduction of oxygen in the potential region from open circuit to −1.2 V (presumably generating hydrogen peroxide) did not significantly affect the OCP of the Al–40% Zn alloy electrode. The onset of hydroxide generation is known to occur close to −1.2 V, and this resulted in a substantial negative shift in the OCP of the alloy, which correlated with the polarisation data for the heat-treated Al–40% Zn alloy in alkaline electrolyte. The apparent delay in the change of OCP observed between the arrays spaced at 10, 50 and 200 μm appeared to be related to the diffusion time across the electrode gap, while the magnitude of the change in potential was related to the difference in hydroxide concentration at the surface.

In contrast, cathodic polarisation of one of the zinc bands using the other zinc band in the array as the counter electrode resulted in the OCP of the Al–40% Zn alloy remaining around −0.95 V for closely spaced arrays. This result illustrates the importance of the interaction between the generated species at the anodic and cathodic sites. Presumably, the pH change in the vicinity of the Al–40% Zn alloy with the working and counter electrodes closely spaced was much less. It is plausible that during the dissolution of zinc at the anode, the pH is decreased over the region encompassing all electrodes and that Zn^{2+} reduction at the cathode contributed to the cathodic current, effectively lowering the rate of oxygen reduction.

During potential step experiments where both zinc bands were polarised to −1.4 V to generate hydroxide, the magnitude of the negative shift in OCP for the Al–40% Zn alloy in the arrays spaced at 10 and 50 μm is likely to be representative of the concentration of hydroxide at the surface. The positive drift in the OCP of the alloy in the array spaced at 200 μm during the zinc potential step reflects the smaller impact of pH change at this band separation and the underlying behaviour of the alloy to change to a more positive potential in this electrolyte, as observed for the largely spaced electrodes. The behaviour of the OCP of the alloy in the closely spaced arrays on cessation of hydroxide generation suggests that the electrolyte near the surface tended to return to neutral pH. However, the OCP of the heat-treated alloys did not attain the values measured for the largely spaced electrodes, indicating that the surface of the alloy was altered by exposure to the alkaline conditions.

The difference in behaviour observed in the galvanic couple experiments between electrodes spaced at 10, 50 and 200 μm and those far apart is attributed to the mass transport and interaction of ions arising from cathodic and anodic processes. The intersection of the polarisation curves suggests that the heat-treated Al–40% Zn alloy would act as a cathode and the zinc as an anode in neutral Na_2SO_4 electrolyte with a galvanic current of 5 μA cm^{-2}. This was observed in cells with large inter-electrode spacing soon after coupling. The arrays with small inter-electrode spacing differ from the predicted behaviour because of interacting anodes and cathodes, producing significantly different conditions under which the polarisation curves were recorded. The cell potentials for the bulk of the galvanic couple period were close to the E_{corr} of zinc in Na_2SO_4 and NaCl electrolytes, suggesting that the bulk of the galvanic current arose from oxygen reduction and zinc dissolution.

The polarisation experiments on the BME arrays demonstrate that varying degrees of diffusional overlap occur at 10, 50 and 200 μm spacings. The similarity of the galvanic behaviour between these arrays suggested that the degree of interaction did not significantly affect the overall galvanic behaviour of the cells. The more negative cell potential observed for the 10- and 50-μm-spaced arrays in the first 4 h of coupling may be attributed to the interaction of the reaction products originating from the bands, but this did not appear to affect the galvanic current. Inspection of the electrode surfaces following the galvanic coupling experiments suggested that galvanic cells were established along the band length in addition to between the bands. This localised effect has the potential to further complicate the behaviour of the arrays and make the interpretation of the results less straightforward. In summary, these results demonstrate that the inter-electrode spacing the bands has a significant effect on the overall behaviour of the array; however, studies into the intra-band processes are required to understand these observations.

Conclusion

Electrochemical polarisation experiments have shown that anodic dissolution processes on Al–40% Zn alloys are significantly enhanced in chloride compared to sulfate-based electrolytes. The aluminium content of the alloys allowed passive behaviour to be observed even in the presence of zinc-rich precipitates on the surface of an alloy. Electrolyte pH affected the cathodic processes, which may be attributed to the rate of proton reduction and the passivity of the surface. Polarisation experiments while monitoring the OCP of neighbouring electrodes in BME arrays showed that generation of alkaline pH at zinc electrodes may influence the environment at neighbouring array elements located 10, 50 and 200 μm away. Where the elements of a BME array interact via mass transport of zinc ions and products of oxygen reduction, the overall galvanic behaviour of the cell may be

anodic or cathodic rather than the alloy strictly being the cathode as observed for largely spaced electrodes.

Acknowledgements The authors are grateful for financial support from the Australian Research Council. The authors sincerely appreciate the technical advice given by D. Nolan and the assistance of A. McCulloch in obtaining the SEM images.

References

1. Townsend HE (1999) Corrosion 55:547
2. Zhang XG (1996) J Electrochem Soc 143:1472. doi:10.1149/1.1836662
3. Townsend HE (1998) Corrosion 54:561
4. Cole IS, Neufeld AK, Furman S, Sherman N (2000) In *198th Electrochemical Society Meeting*; The Electrochemical Society Proceedings Series, Pennington, NJ: Phoenix, Vol. PV2000-23
5. Ramus Moreira A, Panossian Z, Camargo PL, Ferreira Moreira M, da Silva IC, Ribeiro de Carvalho JE (2006) Corros Sci 48:564. doi:10.1016/j.corsci.2005.02.012
6. Elvins J, Spittle JA, Worsley DA (2003) Corros Eng Sci Technol 38:197. doi:10.1179/147842203770226924
7. Nogueira TMC, Cruz MAS, Rios PR (2001) J Mater Eng Perform 10:314. doi:10.1361/105994901770345024
8. Marder AR (2000) Prog Mater Sci 45:191. doi:10.1016/S0079-6425(98)00006-1
9. Palma E, Puente JM, Morcillo M (1998) Corros Sci 40:61. doi:10.1016/S0010-938X(97)00112-1
10. Huafei L, Jiashen Z, Dunyi Y (2001) Mater Perform 40:32
11. Neufeld AK Cole IS (2000) In *198th Electrochemical Society Meeting*; The Electrochemical Society Proceedings Series, Pennington, NJ: Phoenix, Vol. PV2000-25
12. Neufeld AK Cole IS (1996) In *13th International Corrosion Congress* Melbourne
13. El-Mahdy GA, Nishikata A, Tsuru T (2000) Corros Sci 42:1509. doi:10.1016/S0010-938X(00)00009-3
14. Yadav AP, Katayama H, Noda K, Masuda H, Nishikata A, Tsuru T (2007) Electrochim Acta 52:2411. doi:10.1016/j.electacta.2006.08.050
15. McMurray HN (2001) Corrosion 57:313
16. Worsley DA, McMurray HN, Sullivan JH, Williams IP (2004) Corrosion 60:437
17. McMurray HN, Parry G, Jeffs BD (1998) Ironmak Steelmak 25:210
18. Dafydd H, Worsley DA, McMurray HN (2005) Corros Sci 47:3006. doi:10.1016/j.corsci.2005.05.036
19. Miao W, Cole IS, Neufeld AK, Furman S (2007) J Electrochem Soc 154:C7. doi:10.1149/1.2372691
20. Deslouis C, Duprat M, Tulet-Tournillon C (1984) J Electroanal Chem 181:119. doi:10.1016/0368-1874(84)83624-2
21. Birbilis N, Buchheit RG (2005) J Electrochem Soc 152:B140. doi:10.1149/1.1869984
22. Scully JR, Knight TO, Buchheit RG, Peebles DE (1993) Corros Sci 35:185. doi:10.1016/0010-938X(93)90148-A
23. Liao CM, Wei RP (1999) Electrochim Acta 45:881. doi:10.1016/S0013-4686(99)00299-6
24. Idrac J, Mankowski G, Thompson G, Skeldon P, Kihn Y, Blanc C (2007) Electrochim Acta 52:7626. doi:10.1016/j.electacta.2007.05.056
25. Mujibur Rahman ABM, Kumar S, Gerson AR (2008) Corros Sci 50:1267. doi:10.1016/j.corsci.2007.11.035
26. Aballe A, Bethencourt M, Botana FJ, Cano MJ, Marcos M (2003) Corros Sci 45:161. doi:10.1016/S0010-938X(02)00067-7
27. Campestrini P, van Westing EPM, van Rooijen HW, de Wit JHW (2000) Corros Sci 42:1853. doi:10.1016/S0010-938X(00)00002-0
28. Aoki K, Tokuda K, Matsuda H (1987) J Electroanal Chem 225:19. doi:10.1016/0022-0728(87)80002-5
29. Saito Y (1968) Rev Polarog 15:177
30. Aoki K, Tokuda K, Matsuda H (1987) J Electroanal Chem 230:61. doi:10.1016/0022-0728(87)80131-6
31. Cope DK, Scott CH, Kalapathy U, Tallman DE (1990) J Electroanal Chem 280:27. doi:10.1016/0022-0728(90)87081-T
32. Alden JA, Booth J, Compton RG, Dryfe RAW, Sanders GHW (1995) J Electroanal Chem 389:45. doi:10.1016/0022-0728(95)03923-5
33. Britz D, Poulsen K, Strutwolf J (2005) Electrochim Acta 51:333. doi:10.1016/j.electacta.2005.04.030
34. Deakin MR, Wightman RM, Amatore CA (1986) J Electroanal Chem 215:49. doi:10.1016/0022-0728(86)87004-8
35. Aoki K, Tanaka M (1989) J Electroanal Chem 266:11. doi:10.1016/0022-0728(89)80211-6
36. Seddon BJ, Girault HH (1989) J Electroanal Chem 266:227. doi:10.1016/0022-0728(89)85070-3
37. Aoki K (1990) J Electroanal Chem 284:35. doi:10.1016/0022-0728(90)87060-W
38. Fosset B, Amatore C, Bartelt J, Wightman RM (1991) Anal Chem 63:1403. doi:10.1021/ac00014a012
39. Arkoub IA, Amatore C, Sella C, Thouin L, Warkocz JS (2001) J Phys Chem B 105:8694. doi:10.1021/jp010764g
40. Ferrigno R, Josserand J, Brevet PF, Girault HH (1998) Electrochim Acta 44:587. doi:10.1016/S0013-4686(98)00187-X
41. Harriman K, Gavaghan DJ, Houston P, Suli E (2000) Electrochem Commun 2:567. doi:10.1016/S1388-2481(00)00074-6
42. Amatore C, Oleinick AI, Svir IB (2003) J Electroanal Chem 553:49. doi:10.1016/S0022-0728(03)00269-9
43. Morf WE, Koudelka-Hep M, de Rooij NF (2006) J Electroanal Chem 590:47. doi:10.1016/j.jelechem.2006.01.028
44. Streeter I, Fietkau N, delCampo J, Mas R, Munoz FX, Compton RG (2007) J Phys Chem C 111:12058. doi:10.1021/jp073224d
45. Oldham KB (1981) J Electroanal Chem 122:1
46. Szabo A, Cope DK, Tallman DE, Kovach PM, Wightman RM (1987) J Electroanal Chem 217:417. doi:10.1016/0022-0728(87)80233-4
47. Wipf DO (1994) Colloids Surf A Physicochem Eng Asp 93:251. doi:10.1016/0927-7757(94)02872-9
48. Davoodi A, Pan J, Leygraf C, Norgren S (2005) Electrochem Solid-State Lett 8:B21. doi:10.1149/1.1911900
49. Davoodi A, Pan J, Leygraf C, Norgren S (2006) Appl Surf Sci 252:5499. doi:10.1016/j.apsusc.2005.12.023
50. Vignal V, Krawiec H, Heintz O, Oltra R (2007) Electrochim Acta 52:4994. doi:10.1016/j.electacta.2007.01.079
51. Souto RM, Gonzalez-Garcia Y, Bastos AC, Simoes AM (2007) Corros Sci 49:4568. doi:10.1016/j.corsci.2007.04.016
52. Lister TE, Pinhero PJ (2005) Anal Chem 77:2601. doi:10.1021/ac0485785
53. Budiansky ND, Bocher F, Cong H, Hurley MF, Scully JR (2007) Corrosion 63:537
54. Budiansky ND, Hudson JL, Scully JR (2004) J Electrochem Soc 151:B233. doi:10.1149/1.1666168
55. Lunt TT, Scully JR, Brusamarello V, Mikhailov AS, Hudson JL (2002) J Electrochem Soc 149:B163. doi:10.1149/1.1466858
56. Lunt TT, Brusamarello V, Scully JR, Hudson JL (2000) Electrochem Solid-State Lett 3:271. doi:10.1149/1.1391122
57. Van Gheem E, Vereecken J, Le Pen C (2002) J Appl Electrochem 32:1193. doi:10.1023/A:1021656820760
58. Yu SY, O'Grady WE, Ramaker DE, Natishan PM (2000) J Electrochem Soc 147:2952. doi:10.1149/1.1393630
59. McCafferty E (2003) Corros Sci 45:1421. doi:10.1016/S0010-938X(02)00231-7